Growth and characterization of ferroelectric $SrBi_2Ta_2O_9$ single crystals via high-temperature self-flux solution method

© H. Amorín*, I.K. Bdikin*,**, A.L. Kholkin*, M.E.V. Costa*

* Department of Ceramics and Glass Engineering & Center for Research in Ceramic and Composite Materials (CICECO), University of Aveiro, 3810-193 Aveiro, Portugal

** Institute of Solid State Physics, Russian Academy of Sciences, Chernogolovka, Moscow district, 142432 Russia

E-mail: kholkin@cv.ua.pt

(Received Juni 24, 2005)

$SrBi_2Ta_2O_9$ (SBT) single crystals were produced by high temperature self-flux solution method using a Bi_2O_3 flux modified with B_2O_3. The processing conditions were optimized to obtain large and translucent SBT crystals with a layered habit and typical dimensions of approximately $7 \times 5 \times 0.2$ mm. *X*-ray diffraction and *x*-ray topography measurements revealed the major faces of the crystals with natural rectangular platelet morphology are perfectly (001)-orientated with edges directed along the [110] directions. High quality of the crystals was confirmed by rocking curves (half width of 0.04° for the (0 0 18) reflection) and by ferroelectric measurements. The anisotropy in the dielectic and ferroelectric properties was investigated both along the [110] (*ab*-plane) and the [001] (*c*-axis) directions. The growth mechanism, morphology and dielectric anisotropy of the SBT crystal platelets are discussed based on its crystallographic structure.

H. Amorín and I.K. Bdikin acknowledge the Foundation for Science and Technology (FCT, Portugal) for the financial support through Ph.D. and Postdoctoral grants, respectively.

PACS: 77.84.-s, 81.10.-h

1. Introduction

Bi-layered structured ferroelectrics (BLSF) and, particularly, $SrBi_2Ta_2O_9$ (SBT) have been recognized as promising materials for non-volatile ferroelectric random access memories (NvFRAMs) due to their excellent fatigue endurance and low leakage current [1–3]. A large amount of work has been focused of SBT thin films for NvFRAMs, where dramatic improvement of the ferroelectric properties has been achieved using modern deposition techniques. However, these achievements have not been followed by the corresponding understanding of the fundamental properties of SBT that are obviously obscured by the insufficient quality, texture, polycrystallinity and interface problems of the investigated films [4–6]. Therefore the study of single crystal (intrinsic) properties of this material may contribute to further development of memory devices and to improving functionality of SBT films. To date this study has not been done yet because of the lack of large SBT crystals of sufficient quality. Consequently, the optimization of techniques for obtaining large and high-quality SBT single crystals is highly desirable.

Ferroelectric materials have been grown in a single crystal form for a long time with the ultimate goal of comparing their properties with those of polycrystalline materials of identical composition [7–11]. Single crystals are indispensable for studying the anisotropy of ferroelectric and dielectric properties in BLSF systems. In order to perform the measurements, single crystals of sufficiently high quality should be in a single-domain state or, at least, have a controlled domain configuration. However, there were only a few attempts to grow and to characterize large SBT single crystals contrary to some other BLSF compositions [7,8,12–14]. The major problem was due to considerable difficulties in synthesizing SBT single crystals [15–17]. High temperature self-flux solution method is one of the potential techniques suitable for the fabrication of ferroelectric single srystals [18], namely for producing several Pb-based complex perovskites and some BLSF materials, using lead and bismuth oxide fluxes, respectively [7–18]. Such fluxes at high temperature are advantageous because their constituent elements are also a part of the desired final composition, and, therefore, the incorporation of foreing ions into the lattice of the grown crystals is avoided. Moreover, the melting point may be conveniently reduced by adding other component to the flux, i.e., B_2O_3 [17,18]. The main disadvantage of this method is the slow growth rate and the excessive power consumption for growing large crystals.

In BLSF crystals, the perovskite blocks of $A_{m-1}B_mO_{3m+1}$ are interleaved with bismuth oxide (B_2O_2) layers, where m denotes the number of BO_6 octahedral layers in the perovskite blocks [19]. The Bi_2O_2 layers control the SBT electronic response [20], while the dielectric and ferroelectric anisotropy originates from the two-dimensional perovskite-like structure and depend on the value of m (mainly on whether m is even of odd [8,19]). SBT system ($m = 2$) is characterized by the orthorhombic distortion (space group $A2_1an$) in the ferroelectric phase of the tetragonal prototype structure ($I4/mmm$) [21].

In the last years, the efforts were mainly focused on obtaining SBT single crystals by self-flux method using a Bi_2O_3 flux [15,16]. These attempts resulted in crystals too small to be used for further evaluation. Only recently

large SBT single crystals were successfully synthesized using a modified self-flux solution method [17]. However, the structural characteristics of the obtained crystals have not been fully investigated, thus deserving further studies, since they are crucial for determining intrinsic electrical properties of SBT. The main objective of this work was to optimize the processing conditions for the growth of large, high-quality $SrBi_2Ta_2O_9$ single crystals, while reducing the power consumption. The growth mechanism of SBT is descussed based on its crystalline structure. The structural and electrical properties are evaluated and used to confirm the quality of the grown SBT crystals.

2. Experimental procedures

2.1. Single crystal growth parameters. SBT single crystals were grown using a modified high temperature self-flux solution method described elsewhere [18,22]. Polycrystalline SBT powder was firstly synthesized via solid-state reaction using high-purity (> 99.5%) $SrCO_3$, Bi_2O_3 and Ta_2O_5 reagents. These powders were mixed in stoichiometric amounts and placed in a 15 ml Pt crucible tightly sealed with a Pt lid. The Pt crucible was then inserted in a large sealed alumina crucible to minimize the evaporation of Bi. Pure SBT powder was obtained by heating up to 950°C and soaking at this temperature for 2 h in air. After the firing process the powder was ball milled in ethanol for 8 h using zirconia balls in a polyethylene jar and then mixed with the flux using a molar ratio of 60/40 of SBT to flux. The flux used was a mixture of 35 wt.% of Bi_2O_3 (melting point 825°C) and of 5 wt.% of B_2O_3 (melting point 450°C).

An amount of 40 g of the ground SBT/flux mixture was put into a 15 ml Pt crucible (base diameter 2 cm) tightly sealed with a Pt lid. Fig. 1 shows the setup used for the growth of SBT single crystals. The Pt/Al_2O_3 double crucible sealed with alumina cement was used to prevent the evaporation of the flux at high temperture. First, a premelting was done at 950°C for 2 h, followed by the melting and cooling stages using the three different thermal profiles illustrated in Fig. 2. These profiles include heating up to 1350°C and soaking at this temperature for 10 h. After this, a gradually accelerated slow cooling process is introduced in order to create the required supersaturation for crystals nucleation and growth, following one of the three different paths, hereafter TP1, TP2 and TP3. The two first thermal profiles, TP1 and TP2, lasted ~ 4 days, being faster than TP3, a longer profile that allowed for slow cooling for more than a week. This last profile, TP3, was similar to that used by Sih et al. [17]. The profile TP1 included soaking at 1350°C for 10 h, slow cooling down to 1200°C at 5°C/h, which was then changed to 10°C/h down to 1000°C, then to 20°C/h down to 800°C, and finally to 100°C/h down to room temperature. The only difference appearing in the TP2 with respect to the TP1 profile is the inclusion of an initial slow cooling rate of 2°C/h from 1350°C down to 1300°C. After this, the cooling rate was

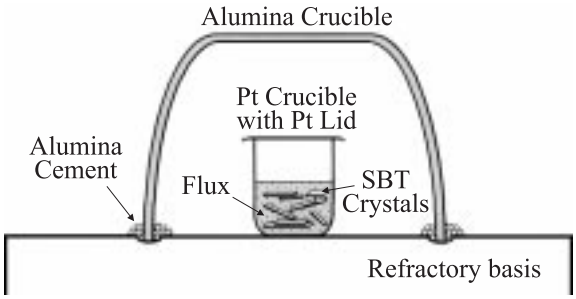

Figure 1. Setup for the growth of $SrBi_2Ta_2O_9$ single crystals by spontaneous nucleation. The assembly of Pt and Al_2O_3 crucibles is used to prevent the evaporation of the flux at high temperature, due to its high volatility.

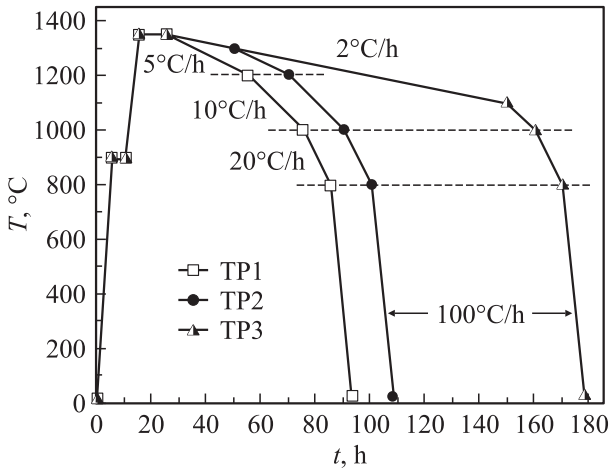

Figure 2. An illustration of the furnace thermal profiles with several slow cooling rates used for the growth of $SrBi_2Ta_2O_9$ single crystals.

increased to 5°C/h, following a parallel path to TP1 profile. In the case of the TP3 profile, an initial slow cooling rate of 2°C/h is extended down to 1100°C, changing to 10°C/h down to 1000°C, then to 20°C/h down to 800°C, and finally to 100°C/h down to room temperature.

After the various growth runs the wieght losses were evaluated. In all cases, the weight losses fluctuated between 15 and 20% of the initial powder amount (flux plus SBT). Since the initial amount of flux was 40 wt.% of the total powder, these losses are believed to be mainly associated with the flux evaporation out from the platinum crucible during the thermal treatments. This fact was also confirmed by the analysis of the quality of the alumina crucible after the various growth runs, where some yellowish coloration in the inner side of the alumina crucible was observed. However, neither the outer side of the alumina crucible nor the alumina cement were found to be visibly colored with yellowish contaminant.

The grown SBT crystals were separated from the flux using a two-step process. First, the crystals and solidified flux were taken out from the Pt crucible by inverting it on a porous ceramic at 1000°C, and then the crystals were

separated by leaching in hot nitric acid to dissolve the flux. This process is slow and takes a few days to completely remove the existing flux between the platelet single crystals. Finally, SBT crystals were leached in hot water for several hours to dissolve the nitric salt and then annealed at 750°C for 10 h.

2.2. Characterization techniques. The evaluation of the grown single crystal structural quality was performed by x-ray angular θ-2θ and θ-scanning topography methods [23,24]. The platelet sample was rotated at an angular rate ω and, for θ-2θ-scanning topography, a photographic film placed directly in front of the x-ray detector and perpendicular to the diffracted beam was rotated at an angular rete 2ω or remained fixed for θ-scanning topography. The standard DRON-2 diffractometer was used. The θ-2θ-scanning topography method is sensitive to misorientation between adjacent blocks of the crystal, and the misorientation angles are related to the angular interval of rotation. It allowed us to produce images from the chosen reflection of all the crystal blocks with misorientation less than the scan interval. The θ-scanning topography does not display the misorientation of the crystallites in the direction of scanning, and only records reflections with different parameters of unit cell. In both cases, the misorientation between crystal blocks around the direction perpendicular to the rotaiton axis of the goniometer is manifested along the vertical direction on the topographs. The samples were also characterized by x-ray diffraction analysis (SIEMENS D500, CuK_α radiation) at room temperature in the 2θ range from 4 to 130° with a step length of 0.02° and the rocking curve was recorded for the (0 0 18) reflection. The top view of the crystal major face was examined using a Zeiss optical microscope with a JVC camera connected to a PC.

For electrical characterization, naturally shaped single crystals were polished in two directions: parallel to the ab-plane for measurements along the c-axis, and perpendicular to the [110] direction for measurements in the ab-plane. Gold electrodes were sputtered onto the whole area of the polished facets. Dielectric properties were measured using a HP4284A LCR Meter and the hysteresis loops were observed using a Sawyer–Tower circuit (frequency 50 Hz) at room temperature.

3. Results and discussion

3.1. Single crystal growth. It has been already known that high-quality SBT single crystals can be obtained by the self-flux solution method adding a low amount of B_2O_3 to the Bi_2O_3 flux [17,25]. Without B_2O_3 addition, the SBT powder does not melt thoroughly at 1350°C due to the high and incongruent melting point of the SBT phase, resulting in crystals with sizes smaller than 0.5 mm, some of them being formed around Pt lid in the vapor phase region and having different phases including SBT, $SrTa_4O_{11}$ and $Sr_2Ta_2O_7$ [16,25,26]. The addition of a small amount of B_2O_3 (5 wt.% in our case) to the flux improves the crystallization by promoting powder melting and leading to a more viscous and stable medium for SBT nucleation. The obtained crystal dimensions for the three thermal profiles and a SBT/flux ratio of 60/40 are summarized in Talbe 1.

Table 1. Results of SBT crystal growth for different thermal profiles

Flux composition, wt.%		Temperature profile	Maximum size, mm^3
Bi_2O_3	B_2O_3		
35	5	TP1	$1 \times 1 \times 0.02$
35	5	TP2	$7 \times 5 \times 0.2$
35	5	TP3	$5 \times 3 \times 0.1$

Large and translucent SBT single crystals with a layered habit and faceted surfaces were obtained with the boron-modified flux. The sizes of the crystals were seen to depend on the used temperature profile. For the first profile (TP1), small crystals were obtained with major face size smaller than 1×1 mm. In contrast, for the other two profiles used (TP2 and TP3), the crystal sizes varied between 5×3 mm for TP3 (dimensions similar to those reported by Sih et al. [17] when using a 2 cm base diameter Pt crucible and the same temperature profile) and 7×5 mm for TP2, with thickness ranging between 50 and 200 μm in both cases. Fig. 3, *a* shows a micrograph of typical SBT crystals grown using the TP2 thermal profile.

It is noteworthy to mention that the longer profile (TP3) with the slowest cooling process did not result in the biggest crystals which were obtained using TP2, a shorter profile as compared to that used by Sih et al. [17]. During the cooling process, supersaturation is created and two distinct phenomena take place: crystal nucleation and crystal growth. For a fixed amount of starting solution, the higher the number of nuclei, the smaller the sizes of the final crystal particles. For the present system, the cooling dependence of the nucleation and growth rates has not been reported so far. These results are believed to result from the competition between these two phenomena. The used combination of temperture and time provided by the TP2 profile creates proper conditions for SBT crystal nucleation and growth, since big SBT crystals were effectively obtained. If the initial cooling is speed up (as in the TP1 profile), much smaller final crystals are found. This behavior may be understood assuming that in this case the initial supersaturation increases and enhances the nucleation rate, giving rise to a larger number of critical nuclei as compared to that formed during the TP2 thermal process. Since both profiles run in parallel after 1300°C, the present results also suggest that the 1300−1350°C temperature range is critical for SBT nucleation. As for the TP3, which produced less developed SBT crystals as compared to TP2, its early stage of crystallization is identical to that of TP2 profile and so the number of nuclei should be similar in both cases. The cooling below 1300°C distinguishes TP2 and TP3 processes, being faster in TP2 and thus promoting in this case a higher initial growth rate of the nucleated crystals [18]. The

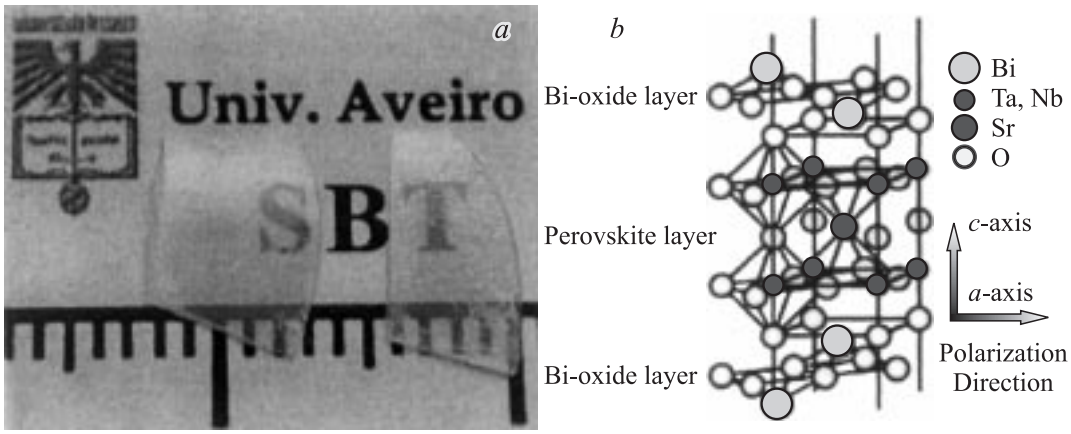

Figure 3. *a* — micrograph showing as-grown and cleaned $SrBi_2Ta_2O_9$ single crystal platelets grown using the TP2 thermal profile. *b* — crystal structure of the layered $SrBi_2Ta_2O_9$ system (pseudoperovskite $SrTa_2O_7$ blocks interleaved with bismuth oxide layers) [21].

slower cooling rate during TP3, while allowing a slower crystal growth, is prone to secondary nucleation events which also contribute to the decrease of supersaturation of the system, thus limiting further crystal growth. To avoid the effect of secondary nucleation, temperature cycling has been proposed as an effective procedure to dissolve smaller crystals.

The growth norphology of a crystal is determined by the internal crystal structure, although, in many cases, the morphology can be also controlled by manipulating the growth parameters (i.e. growth temperature, supersaturation, etc.) [27]. The Hartman–Perdok theory [28] describes the relations between internal crystal structure and crystal morphology. This theory states that the crystal morphology is dominated by the *F* faces, i.e., those containing at least two non-parallel periodic bond chains (PBCs) [29]. The *F* faces are those growing slower according to a layer mechanism, and thus are the only important ones for the crystal morphology. The present results obtained in different supersaturation conditions show that SBT crystal morphology is dominated by [001] facets.

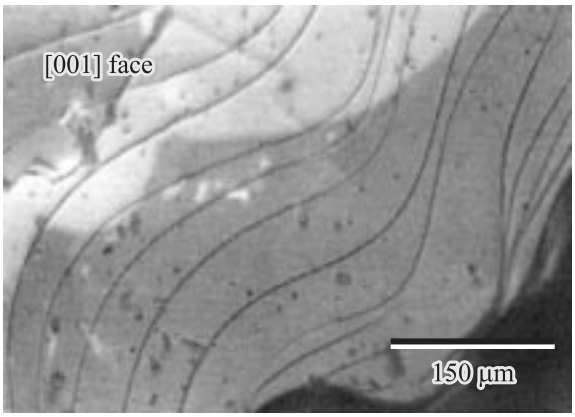

Figure 4. Micro-morphology of the SBT single crystal major face near the crystal edge, showing layered growth steps aligning perpendicular to the [001] direction.

From the point of view of the SBT structure (pseudoperovskite blocks of $SrTa_2O_7$ interleaved with bismuth oxide layers perpendicularly to [001] direction [21], see Fig. 3, *b* for better understanding, the faster growth of the crystals parallel to the *ab*-plane, compared to that along the [100] direction, suggests the existence of PBCs parallel to the *ab*-plane. The application of the PBCs concept to $YBa_2Cu_3O_{7-\delta}$ superconducting single crystals that also have a layered crystalline structure (CuO_2 layered oxygen-deficient perovskites) has predicted a similar growth rate anisotropy, which was experimentally confirmed [27]. Fig. 4 shows the surface micro-mrophological observation of the SBT crystal major face ([001] face) near the crystal edge, revealing growth steps aligned perpendicular to the [001] direction and pointing to a dominant layer growth mechanism for the [001] facets. Further studies are currently underway, aiming a the characterization of the PBCs in the SBT structure as well as of the role of growth parameters (effects of the supersaturation and/or of the temperature of the interfacial kinetics and on the solute diffusion) for determining the final morphology.

3.2. Structural quality of the crystals. The obtained SBT single crystals were characterized by XRD and *x*-ray topography techniques at room temperature. The XRD spectra for a rectangular SBT crystal platelet is shown in Fig. 5, *a, b* where only (*h*00) and (001) plane reflections are observed in the directions parallel and perpendicular to the major face, respectively. Accordingly, highly oriented SBT single crystal platelets (with *c*-axis perpendicular to the major face) were produced. Pseudo-tetragonal lattice parameters were calculated using these data and the orthorhombic space group $A2_1am$ [$a, b \cong 5.508(1)$ Å and $c \cong 25.01(1)$ Å]. These were in a good agreement with the reported data [21,30].

X-ray topography measurements were performed on a small and rectangular shaped crystal with sizes of $2 \times 1 \times 0.02$ mm, approximately. The *x*-ray θ- and θ-2θ-angular scanning topographies are represented in Figs. 6, *a* and 6, *b*, respectively. The θ-angular scanning topograph

Table 2. Dielectric and ferroelectric properties along the [110] (ab-plane) and [001] (c-axis) directions in the $SrBi_2Ta_2O_9$ single crystals: Curie temperature (T_C), room temperature (RT) and maximum permittivitites at 1 MHz, maximum dielectric looses ($\tan\delta$) at 1 MHz, spontaneous polarizations (P_S) and coercive fields (E_C)

Measurement direction	T_C, °C	Permittivity (1 MHz)		Maximum $\tan\delta$ (1 MHz)	P_S, μC/cm^2	E_C, kV/cm
		RT	Maximum			
[110] ab-plane	355	150	1375	0.016	14	22
[001] c-axis	351	110	130	0.012	0	0

in Fig. 6, a was obtained using the (110) reflection. The uniform contrast was observed over all the surface of the sample confirming its perfect orientation. The intensity of this image depends on the thickness of the sample and extinction (defect) crystal conditions. Fig. 6, b represents the diffraction image for θ-2θ-angular scanning topographs using the (0 0 18) reflection. For an ideal crystal this image should correspond to the shape of the sample with a linear transformation governed by the geometry of the experimental setup [23,24]. For the present case, the small deviation of the diffraction image on Fig. 6, b from the real shape (see θ-angular scanning topograph in Fig. 6, a) can be due to small bending of the crystal surface along its major face. Indeed, this deviation is determined by the magnitude of the misorientation, being smaller than 1° for this crystal. The crystal quality is better demonstrated through the rocking curves Fig. 5, c, where the half width of the rocking curve for the (0 0 18) reflection is 0.04° indicating very high quality of the crystals.

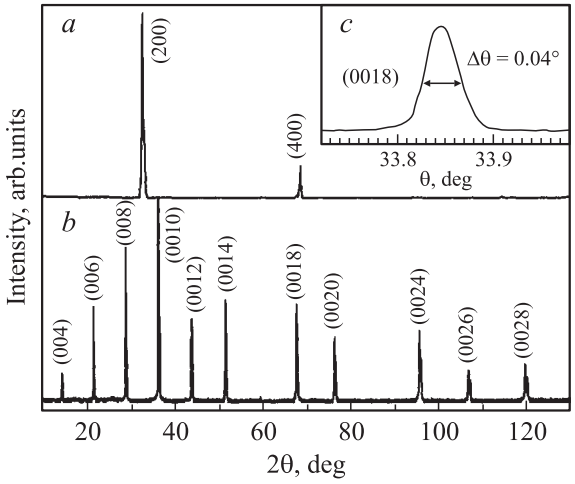

Figure 5. X-ray diffraction spectra for a perfect c-axis oriented SBT single crystal platelet along [100] and [001] directions, respectively (a, b). Rocking curve of the (0 0 18) reflection (c).

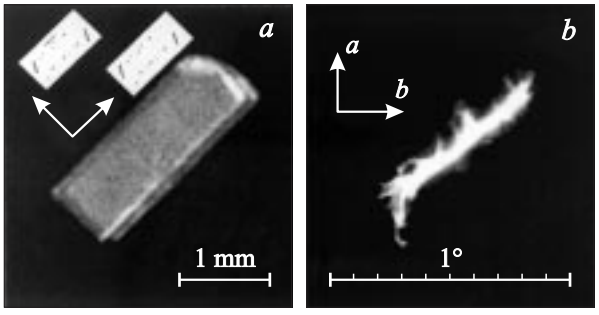

Figure 6. X-ray (a) θ-scanning and (b) θ-2θ-angular scanning topographies, using the (110) and (0 0 18) reflection, respectively, for a small, rectangular and perfect SBT single crystal.

The crystallographic orientation of the SBT single crystal facets can also be deduced from x-ray topography, Fig. 6, a represents the directions of the main crystallographic axes, where the narrow sides of the rectangular shaped crystals are oriented along [110] and [1$\bar{1}$0] directions with the [001] direction (c-axis) lying perpendicular to the major face. As a matter of fact, the shape of the crystals should be determined by the high-symmetry tetragonal phase (space-group $I4/mmm$, $a = b \cong 3.85$ Å) [21], since they were grown at high temperature (far above 1000°C). We believe that, when cooled down to room temperature, the symmetry of single crystal transforms from tetragonal into orthorhombic (space group $A2_1am$) but its original shape formed at high temperature is retained. Apparently, during this transformation, a and b axes rotate by 45° relative to the tetragonal axis and the [100] direction in the tetragonal phase becomes the [110] direction in the orthorhombic phase. It can be thus concluded that the edges of our crystals (directed along [110] and [1$\bar{1}$0] directions at room temperature) originate from the high-symmetry [100] and [010] directions of the tetragonal structure.

3.3. Ferroelectric properties. The anisotropy in the dielectric and ferroelectric properties of the grown SBT single crystals was recently investigated and reported in detail in a separate publication [31]. Table 2 summarizes the results obtained from the permittivity and dielectric losses data as well as from the hysteresis loop measurements both along [110] (ab-plane) and [001] (c-axis) directions. The maximum of dielectric permittivity obtained at $T_C = 355$°C (Curie temperature) is in a good agreement with previous reports on SBT crystals based on XRD, Raman and specific heat measurements [32–34]. It is worth noting that the Curie temperature reported for SBT ceramics (~ 300°C) is somewhat lower than those obtained for single crystals [19,30]. The maximum permittivity of SBT in the ab-plane was about one order of magnitude greater than that along the c-axis, in line with the results obtained in other BLSF single crystals [35]. This value exceeds significantly the corresponding dielectric peak measured in SBT ceramics [19,30]. On the other hand, the low dielectric

looses observed in both cases (along the ab-plane and c-axis ($\tan\delta \leq 0.02$)) confirm the low conductivity of the grown single cyrstals, and thus, the low amount of associated defects and high quality of the crystals.

The values of the spontaneous polarization, P_S, and of the coercive field, E_C, along the [110] direction (ab-plane) were evaluated from the saturated $P-E$ hesteresis loops: $P_S \approx 14\,\mu\text{C/cm}^2$ and $E_C \approx 22\,\text{kV/cm}$. Furthermore, a linear $P-E$ behavior with vanishing remnant polarization was obtained along the [001] direction (c-axis). This is an expected result since for BLSF materials with even number (m) of BO_6 octahedra, the dipole moments caused by ionic displacements along the c-axis are cancelled out due to the presence of a mirror plane perpendicular to the axis [8]. Therefore, in the SBT structure, the spontaneous polarization vector lies entirely along the crystallographic a-axis (in the ab-plane) and no polarization is obtained along the c-axis [30]. In addition, we found that the grown crystals can withstand a high applied electric field ($\sim 60\,\text{kV/cm}$). This confirms again the low concentration of defects contributing to conductivity and electrical breakdown in our crystals.

4. Conclusions

Highly oriented and translucent $SrBi_2Ta_2O_9$ single crystal platelets with layered habit were produced by high temperature self-flux solution method using a boron-modified Bi_2O_3 flux. The largest crystals with sizes around $7 \times 5\,\text{mm}$ and thickness of $200\,\mu\text{m}$ were obtained by an optimized thermal profile that included an accelerated slow cooling process. The anisotropic growth rate of the SBT single crystals was correlated to its crystallographic structure. The narrow sides of the rectangular shaped crystals were oriented along the [110] and [1$\bar{1}$0] directions of the orthorhombic phase with the [001] direction (c-axis) lying perpendicular to the major face.

The high-quality of the grown SBT crystals was also confirmed by the dielectric and ferroelectric measurements. The Curie temperature was observed at $T_C = 355^\circ\text{C}$, while the maximum permittivity measured in the ab-plane was one order of magnitude greater than that along the c-axis. Dielectric losses were lower than 0.02 in the entire temperature range and a high breakdown field was achieved, indicating a low concentration of defects in the single crystals. The spontaneous polarization ($\approx 14\,\mu\text{C/cm}^2$) and coercive field ($\approx 22\,\text{kV/cm}$) were evaluated from the saturated $P-E$ hysteresis loop along the [110] direction (ab-plane), while a linear $P-E$ behavior with vanishing remnant polarization was obtained along the [001] direction (c-axis).

References

[1] C.A. Paz de Araujo, J.D. Cuchiaro, L.D. McMillan, M.C. Scott, J.F. Scott. Nature **374**, *6523*, 627 (1995).
[2] J.F. Scott, F.M. Ross, C.A. Paz de Araujo, M.C. Scott, M. Huffman. Mater. Res. Soc. Bull. **21**, *7*, 33 (1996).
[3] O. Auciello, J.F. Scott, R. Ramesh. Physics Today **51**, *7*, 22 (1998).
[4] K. Amanuma, T. Hase, Y. Miyasaka. Appl. Phys. Lett. **66**, *2*, 221 (1995).
[5] R. Dat, J.K. Lee, O. Auciello, A.I. Kingon. Appl. Phys. Lett. **67**, *4*, 572 (1995).
[6] P.Y. Chu, R.E. Jones, P. Zurcher, D.J. Taylor, B. Jiang, S.J. Gillespie, Y.T. Lii, M. Kottke, P. Fejes, W. Chen. J. Mater. Res. **11**, *5*, 1065 (1996).
[7] S.E. Cummins, L.E. Cross. J. Appl. Phys. **39**, *5*, 2268 (1968).
[8] R.E. Newnham, R.W. Wolfe, J.F. Dorrian. Mater. Res. Bull. **6**, *10*, 1029 (1971).
[9] R. Clarke, R.W. Whatmore. J. Crystal Growth **33**, *1*, 29 (1976).
[10] N. Setter, L.E. Cross. J. Crystal Growth **50**, *2*, 555 (1980).
[11] B.N. Sun, R. Boutellier, Ph. Sciau, E. Burkhardt, V. Rodriguez, H. Schmid. J. Crystal Growth **112**, *1*, 71 (1991).
[12] S.K. Kim, M. Miyayama, H. Yanagida. J. Ceram. Soc. Jpn. **102**, *8*, 722 (1994).
[13] H. Irie, M. Miyayama, T. Kudo. J. Appl. Phys. **90**, *8*, 4089 (2001).
[14] R. Aoyagi, H. Takeda, S. Okamura, T. Shiosaki. Mater. Res. Bull. **38**, *1*, 25 (2003).
[15] M. Susaki, N. Nagasawa, A. Machida, T. Ami. Jpn. J. Appl. Phys. **35**, *5A*, L564 (1996).
[16] A. Machida, N. Nagasawa, T. Ami, M. Suzuki. Jpn. J. Appl. Phys. **37**, *2A*, 795 (1999).
[17] B. Sih, J. Tang, M. Dong, Z.-G. Ye. J. Mater. Res. **16**, *6*, 1726 (2001).
[18] D. Elwell, H.J. Shell. Crystal Growth from High Temperature Solution. Academic Press, N.Y. (1975). Vol. 3. 634 p.
[19] E.C. Subbarao. J. Phys. Chem. Sol. **23**, 665 (1962).
[20] J. Robertson, W. Chen, W.L. Warren, C.D. Gutleben. Appl. Phys. Lett. **69**, *12*, 1704 (1996).
[21] A.D. Rae, J.G. Thompson, R.L. Withers. Acta Crystalogr. Sec. B **48**, *4*, 418 (1992).
[22] W. Tolksdorf. Handbook of Crystal Growth: Bulk Crystal Growth, Flux Growth / Ed. D.T.J. Hurle. Elsevier Science B.V., North Holland (1994). Vol. 2. N 10. P. 563.
[23] I.K. Bdikin, I.M. Shmytko, A.M. Balbashov, A.V. Kazansky. J. Appl. Crystallogr. **26**, 71 (1993).
[24] I. Bdikin, A. Maljuk, S. Watauchi, I. Tanaka, G. Emel'chenko. Physica C **336**, *3–4*, 244 (2000).
[25] H. Amorin, M.E.V. Costa, A.L. Kholkin, J.L. Baptista. J. Eur. Ceram. Soc. **24**, *6*, 1535 (2004).
[26] N. Nagasawa, A. Machida, A. Ami, M. Suzuki. J. Ceram. Soc. Jpn. **106**, *5*, 477 (1998).
[27] Y. Shiohara, A. Endo. Mater. Sci. Eng. R **19**, *1–2*, 1 (1997).
[28] P. Hartman. Crystal Growth: An Introduction. North–Holland, Amsterdam (1973). 531 p.
[29] R.F.P. Grimbergen, H. Meekes, P. Bennema, C.S. Strom, L.J.P. Vogels. Acta Crystallogr. Sec. A **54**, *4*, 491 (1998).
[30] Y. Shimakawa, Y. Kubo, Y. Nakagawa, S. Goto, T. Kamiyama, H. Asano, F. Izumi. Phys. Rev. B **61**, *10*, 6559 (2000).
[31] H. Amorin, V.V. Shvartsman, A.L. Kholkin, M.E.V. Costa. Appl. Phys. Lett. **85**, *23*, 5667 (2004).
[32] S. Kamba, J. Pokorny, V. Porokhonsky, J. Petzelt, M.P. Moret, A. Garg, Z.H. Barber, R. Zallen. Appl. Phys. Lett. **81**, *6*, 1056 (2002).
[33] A. Onodera, K. Yoshio, H. Yamashita. Jpn. J. Appl. Phys. **42**, *9B*, 6218 (2003).
[34] J.-H. Ko, A. Hushur, S. Kojima, B.C. Sih, Z.G. Ye. Appl. Phys. Lett. **81**, *21*, 4043 (2002).
[35] H. Irie, M. Miyayama. Appl. Phys. Lett. **79**, *2*, 251 (2001).